



HAL
open science

Which anatomical directions to quantify local right ventricular strain in 3D echocardiography?

Maxime Di Folco, Thomas Dargent, Gabriel Bernardino, Patrick Clarysse,
Nicolas Duchateau

► To cite this version:

Maxime Di Folco, Thomas Dargent, Gabriel Bernardino, Patrick Clarysse, Nicolas Duchateau. Which anatomical directions to quantify local right ventricular strain in 3D echocardiography?. 12th International Conference on Functional Imaging and Modeling of the Heart, Jun 2023, Lyon, France. pp.607-615. hal-04096724

HAL Id: hal-04096724

<https://hal.science/hal-04096724>

Submitted on 13 May 2023

HAL is a multi-disciplinary open access archive for the deposit and dissemination of scientific research documents, whether they are published or not. The documents may come from teaching and research institutions in France or abroad, or from public or private research centers.

L'archive ouverte pluridisciplinaire **HAL**, est destinée au dépôt et à la diffusion de documents scientifiques de niveau recherche, publiés ou non, émanant des établissements d'enseignement et de recherche français ou étrangers, des laboratoires publics ou privés.



Distributed under a Creative Commons Attribution 4.0 International License

Which anatomical directions to quantify local right ventricular strain in 3D echocardiography?

Maxime Di Folco^{1,2}, Thomas Dargent^{1,3}, Gabriel Bernardino^{1,4}, Patrick Clarysse¹, and Nicolas Duchateau^{1,5}

¹ Univ Lyon, Université Claude Bernard Lyon 1, INSA-Lyon, CNRS, Inserm, CREATIS UMR 5220, U1294, F-69621, Lyon, France

² Institute of Machine Learning in Biomedical Imaging, Helmholtz Munich, Munich, Germany

³ Laboratoire de Météorologie Dynamique (UMR8539), École Polytechnique, IPSL, CNRS, Palaiseau, France

⁴ BCNmedtech, DTIC, Universitat Pompeu Fabra, Barcelona, Spain

⁵ Institut Universitaire de France (IUF)

Abstract Technological advances in image quality and post-processing have led to the better clinical adoption of 3D echocardiography to quantify cardiac function. However, the right ventricle (RV) raises specific challenges due to its specific half-moon shape, which led to a lack of consensus regarding the estimation of RV motion and deformation locally. In this paper, we detail three ways to estimate local anatomically-relevant directions at each point of the RV surface, in 3D, and the resulting Green-Lagrange strain projected along these directions. Using a database of RV surface meshes extracted from 3D echocardiographic sequences from 100 control subjects, we quantified differences between these strategies in terms of local anatomical directions and local strain, both at the individual and population levels. For the latter, we used a specific dimensionality reduction technique to align the latent spaces encoding the strain patterns obtained from different computations of the anatomical directions. Differences were subtle but visible at specific regions of the RV and partially interpretable, although their impact on the population latent representation was low, which sets a preliminary quantitative basis to discuss these computation standards.

Keywords: Cardiac imaging ; right ventricle ; 3D echocardiography ; myocardial strain ; standardization.

1 Introduction

Assessing the cardiac function is complex given the variety of factors affecting the heart geometry and its dynamics. Three-dimensional quantification of its shape and deformation is particularly relevant for the right ventricle (RV), given its asymmetric shape not properly captured with standard 2D imaging planes [1]. Myocardial strain can be decomposed along three orthogonal directions (radial, circumferential, and longitudinal) related to the local arrangement of fibers

within the myocardium, and undergoes specific changes along these directions depending on disease. However, this local assessment remains complex and sensitive to differences in computations. As a result, for echocardiography, clinical studies focus on global or regional assessment in 2D and mostly along the longitudinal direction, which may be critical to detect subtle abnormalities related to disease.

Despite recent promising post-processing of 3D echocardiographic sequences of the RV [2], there is currently no standard for the definition and computation of anatomical directions for the RV [3] and therefore local directional strain, contrary to the left ventricle (LV) [4]. A group of authors proposed to decompose cardiac motion along global axes aligned to its main dimensions [5,6]. Other works used local anatomical coordinates to decompose deformation, defining the longitudinal and circumferential directions from the long-axis and radial directions [7]. Coordinates-independent analysis was also proposed by considering principal strain, obtained by eigendecomposition of the strain tensor [8].

In this paper, we detail three relevant strategies to estimate local anatomical directions over the RV in 3D echocardiography, two of them not being implemented in the literature. Furthermore, we quantify their differences and impact on local strain computations against the RV geometry, both at the individual and population levels, with the underlying aim to foster discussion around such standards.

2 Methods

2.1 Data and pre-processing

We processed RV surface meshes from 100 control subjects, obtained from semi-automatic endocardial segmentation by an expert clinician and tracking of 3D echocardiographic sequences using commercial software (4D RV Function 2.0, TomTec Imaging Systems GmbH, Germany), and exported for post-processing as VTK files. These meshes consisted of 822 points and 1587 triangular cells, after cropping out the tricuspid and pulmonary valves. Point-to-point mesh correspondences were provided by the commercial software, allowing comparisons between subjects at each location of the RV surface. We also realigned them across the population using generalized Procrustes analysis with a rigid transform.

In the following, the local directions and strain are defined at each cell of the RV surface mesh. The radial direction is defined as the normal to the RV surface at each point. We therefore focus explanations on the other two directions: longitudinal and circumferential.

2.2 Estimation of circumferential and longitudinal directions

Long-axis method: The first implemented method (Fig.1a) uses the long-axis, which joins the apex and the basal point equidistant from the valves centers.

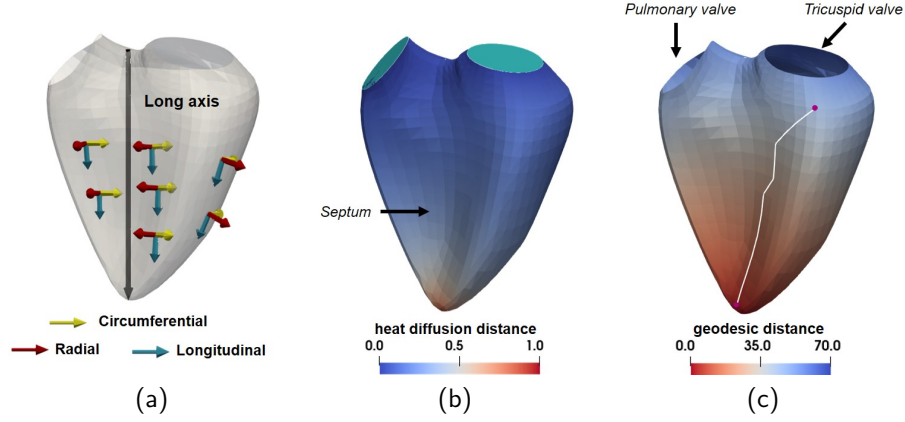


Figure 1: The three ways to compute circumferential and longitudinal directions we evaluated in this paper. (a) Long-axis computations, (b) Heat diffusion computations (the turquoise disks represent the cold point, while the apex stands as the hot point), (c) Geodesic distance computations (the white line corresponds to the geodesic joining the two purple dots).

The circumferential direction is obtained locally from the cross product between the radial direction and the long-axis, then the longitudinal direction is obtained from the cross product between the radial and circumferential directions, as reported in [7].

The RV is actually bi-axial, considering the axes joining the apex and the center of each valve ; the single axis definition is therefore not fully anatomically-relevant. In other words, the longitudinal direction estimated with this approach is a rough approximation.

Heat diffusion method: This method estimates the longitudinal direction as the gradient of the map u , which is defined by solving the following partial differential equation:

$$\nabla \cdot (\nabla u) = 0. \quad (1)$$

This corresponds to the stationary solution of a diffusion process from hot to cold points, which in our case were set to the apex ($u = 1$) and the valves ($u = 0$), respectively (Fig.1b). The map u can be estimated iteratively, by (at each iteration) setting the value at each point as the weighted average of the values at neighboring points in the graph defined by the RV mesh, updating all points, and then restoring the original values 1 and 0 to the apex and the valves. An alternative can be to find a direct solution using the Laplace Beltrami operator. Once the longitudinal direction is estimated, the circumferential direction is computed as the cross product between the radial and longitudinal directions.

Geodesic distance method: This method defines the longitudinal direction as the gradient of the geodesic distance to the apex (Fig.1c), and again the cir-

cumferential direction as the cross product between the radial and longitudinal directions. A first option to compute the geodesics consists of a shortest path algorithm such as Dijkstra’s, on the graph defined by the mesh points. However, this method uses paths that do not go through the mesh cells but along the cell edges, and therefore roughly approximate the geodesics. To overcome this, we used an exact computation of the surface geodesics [9], which gives geodesics that do not necessarily follow the cell edges.

2.3 Computation of longitudinal and circumferential strain

Once the local directions are computed, the local strain tensor is estimated as the Green Lagrangian strain:

$$\mathbf{E} = \frac{1}{2}(\mathbf{J}^T \cdot \mathbf{J} - \mathbf{I}), \quad (2)$$

where $\mathbf{J} = \nabla v + \mathbf{I}$, with ∇v the displacement gradient at a given point, and \mathbf{I} is the identity matrix.

Then, longitudinal and circumferential directional strains are obtained by projecting the strain tensor along these two directions, as:

$$\mathbf{E}_{\mathbf{h}} = \mathbf{h}^T \cdot \mathbf{E} \cdot \mathbf{h}, \quad (3)$$

where \mathbf{h} is the unit vector defining the considered direction. As only endocardial meshes were available due to the thin RV myocardial wall, the radial strain was not computed.

This slightly differs from the computations in [7], which estimated the relative change of length of $5mm$ segments along each anatomical direction separately. Although equivalent in theory for uni-axial deformation, the Green Lagrangian strain is better defined in practice (computations based on the gradient, and not on a direction whose definition may be arguable).

In our database, all the strain patterns were available at each point of the RV surface and at each instant of the cycle. Nonetheless, we focused the evaluation on end-systolic strain patterns, of higher magnitude. In all figures, results are displayed on end-diastolic meshes, which better render anatomical differences between subjects before deformation.

2.4 Quantifying differences in strain patterns

For each individual, we first quantified the point-to-point differences between the anatomical directions estimated with each of the three methods described above, and between the strain values obtained from these directions. The Euclidean norm was used to compute such differences.

We also performed comparisons at the population level, by examining the latent spaces encoding the strain patterns, obtained by a specific dimensionality reduction technique that performs latent space alignment (multiple manifold

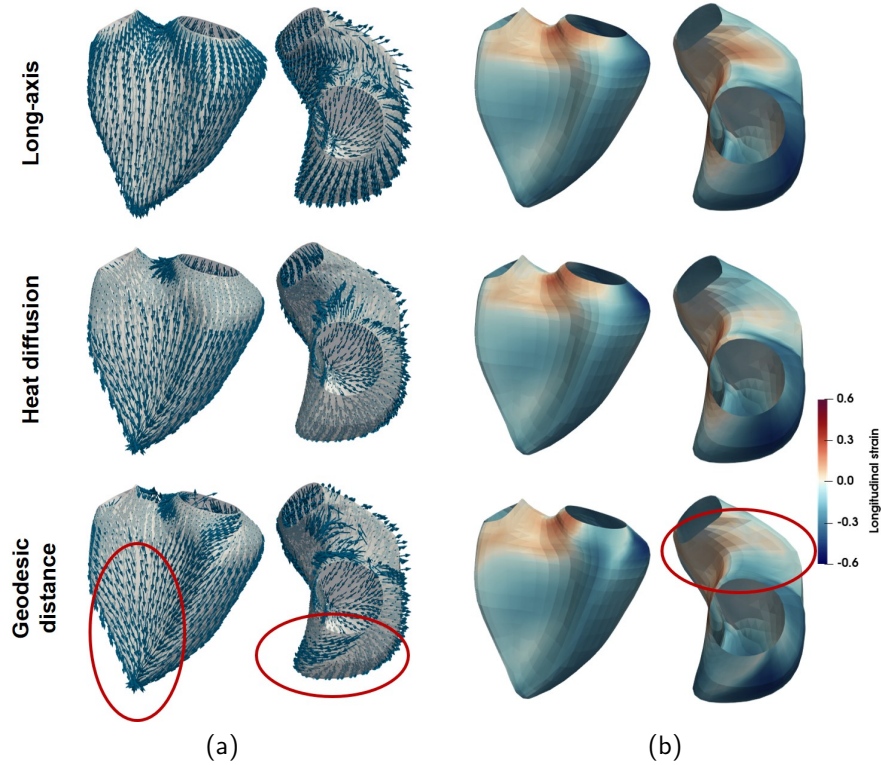


Figure 2: Illustration on a representative case of the local differences (displayed on the end-diastolic mesh / septal and basal views, respectively) in (a) the longitudinal directions, and (b) the resulting end-systolic strain, in %, for the three different computations: long-axis, heat diffusion and geodesic distance.

learning (MML) algorithm, as used in [10]). We fed this algorithm with longitudinal strain obtained by the long-axis method and either the heat diffusion or the geodesic distance method, for the whole population. Dimensionality reduction in MML is based on a generalization of the Laplacian eigenmaps framework [11] to several descriptors. It estimates a latent space for each descriptor, and simultaneously brings together in the latent space samples for which the descriptors are close (regarding a given sample and its neighbors). This is relevant to examine for which samples in the population the strain computations differ and their impact on a low-dimensional representation of the population.

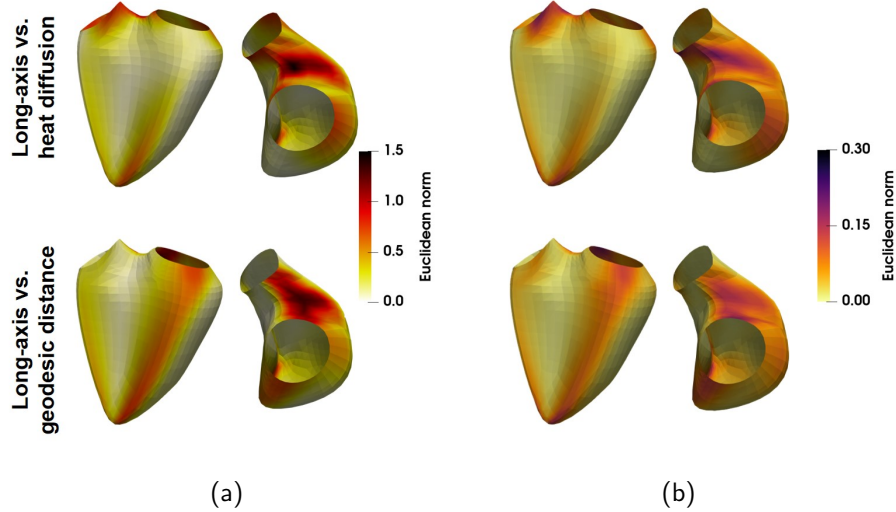


Figure 3: Average local differences across the population (displayed on the end-diastolic mesh / septal and basal views, respectively) in (a) the longitudinal directions, in mm , and (b) the resulting end-systolic strain, in $\%$, for the heat diffusion (top row) and the geodesic distance (bottom row) methods compared to the long-axis one. The Euclidean norm was used to compute such differences.

3 Experiments and results

3.1 Local differences

We first examined local differences regarding the anatomical directions and strain. Figure 2 illustrates this on a representative individual. Only the longitudinal direction and longitudinal strain are displayed to remain concise.

The three methods observed independently provide directions that may sound plausible. However, differences in the longitudinal direction are visible between the long-axis method and the two other methods on the RV septum, in particular near the apex where the former tends to be straight, while the other two tend to point at the apical point (see red circle in the first column). The geodesic distance method is rather sensitive to local specificities of the RV shape, namely that the shortest path taken to reach the apex is not exactly what one might (wrongly) imagine, in particular near the valves (see red circle in the second column). These differences mostly impact strain computations near the valves, where differences in the directions are combined to smaller and more elongated triangular cells, and where segmentation and tracking are also more challenging.

Figure 3 complements these observations by showing the average differences in the longitudinal direction and longitudinal strain across the whole population (long-axis method compared to the other two), displayed over the average mesh

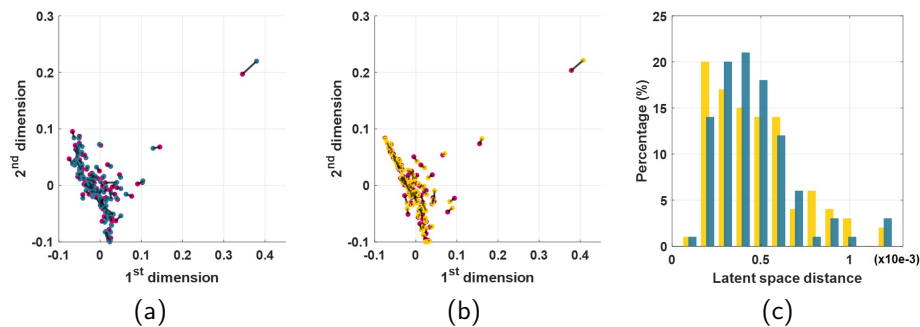


Figure 4: Latent space estimated by manifold alignment (MML algorithm) for (a) the long-axis (in purple) and heat diffusion (in blue) methods or for (b) the long-axis and geodesic distance (in yellow) methods. The black lines join pairs of samples from the same subject. (c) Distribution of distance between samples from the same subject in blue and yellow respectively for the latent spaces in (a) and (b).

across the population. Again, differences are mostly located near the valves. They are much more limited over the RV walls regarding the longitudinal direction, while slight differences are noticed regarding longitudinal strain near the apex at the borders of the septal wall (long-axis vs. the two other methods), and the valve at the borders of septal wall (long-axis vs. geodesic distance method). This corresponds to the observations highlighted with the red circles in Fig.2.

3.2 Population differences

Figure 4 summarizes the distribution of samples in the latent space estimated by MML, fed with the longitudinal strain for the long-axis and heat diffusion methods (Fig.4a), and the long-axis and geodesic distance methods (Fig.4b). Colored dots stand for the distribution of individual samples in the estimated latent space (one color for each method), and black lines join the two samples corresponding to the same subject. The first two dimensions of the latent spaces are displayed. The MML algorithm brings together samples whose input descriptors are close, but does not necessarily bring together samples whose input descriptors differ. Here, we observe that the two latent spaces are rather close, even for individuals a bit out of the distribution, meaning that the different computations of strain have low effect on the analysis of this population. This is confirmed by the histogram of the distances between samples in the two latent spaces (computed across all dimensions).

4 Discussion and conclusion

We have presented three methods to estimate local anatomical directions over the RV, for which no consensus exists in the literature. These directions have been

used to compute local anatomical directions, along which the local strain was computed, in the perspective of analyzing the RV function across the cardiac cycle. On a database of 100 meshes from control subjects obtained from 3D echocardiographic sequences, we have illustrated the differences between these methods on representative subjects and at the population level, and quantified their effect on the analysis of strain patterns using a low-dimensional latent space obtained from MML, a dimensionality reduction technique that performs manifold alignment.

Local differences were observed both on the estimated directions and the strain patterns. These were visible at specific regions (apical septum and near the valves, mainly) and examined against local RV shape specificities for representative individuals. These trends were confirmed by observing these local differences at the population level, but their impact on the latent representation learnt was low and these differences have a minor effect on the main relevant patterns present in the population. This may come from the fact that they only spread across a limited portion of the full RV area, while MML compares subjects across the whole RV (here, using Euclidean distances between the data at all mesh points, considered as a column vector). More differences would be observed by focusing MML on the regions identified in Fig. 3, or with a different metric. Besides, the apex and valve regions are often subject to higher noise and lower image quality, and therefore less reliable for clinical interpretations.

Reaching a consensus to define these anatomical directions, on the specific 3D RV geometry, is challenging. The long-axis method is rather simple to compute but its output may be arguable in particular near the apical septum. The geodesic distance method may seem the most intuitive to match the abstract definition of the longitudinal direction (shortest path to reach the apex), but its output does not seem relevant at specific regions of the RV. The heat diffusion method seems to provide relevant outputs across the whole RV. Computation times were in comparable orders of magnitude for the long-axis ($0.64 \pm 0.01s$ per subject) and geodesic distance ($1.31 \pm 0.03s$) methods, and slightly longer for the heat diffusion method ($4.2 \pm 0.05s$).

Reaching a clear consensus to define such directions should be addressed by our scientific community. Meanwhile, it could be interesting to develop representation learning methods (for the analysis of populations) that could explicitly incorporate several ways to compute a given descriptor (e.g. strain obtained by different methods) and therefore enrich the analysis with such “uncertainties”. We will address this in future work.

Acknowledgements. The authors acknowledge the support from the French ANR (LABEX PRIMES of Univ. Lyon [ANR-11-LABX-0063], the JCJC project “MIC-MAC” [ANR-19-CE45-0005]), and the European Union - NextGenerationEU, Ministry of Universities and Recovery, Transformation and Resilience Plan, through a call from Pompeu Fabra University (Barcelona). They are also grateful to P. Mocerri (CHU Nice, France) for providing the imaging data related to the studied population, and to M. Sermesant (INRIA Epione, Sophia Antipolis, France) for initial discussions on this topic.

References

1. J Sanz, D Sánchez-Quintana, E Bossone, HJ Bogaard, and R Naeije. Anatomy, function, and dysfunction of the right ventricle: JACC state-of-the-art review. *J Am Coll Cardiol*, 73:1463–82, 2019.
2. K Addetia, D Muraru, LP Badano, and Lang RM. New directions in right ventricular assessment using 3-dimensional echocardiography. *JAMA Cardiol*, 4:936–44, 2019.
3. N Duchateau, P Mocerri, and M Sermesant. Direction-dependent decomposition of 3D right ventricular motion: beware of approximations. *J Am Soc Echocardiogr*, 34:201–3, 2021.
4. J D’hooge, A Heimdal, F Jamal, T Kukulski, B Bijmens, F Rademakers, et al. Regional strain and strain rate measurements by cardiac ultrasound: principles, implementation and limitations. *Eur J Echocardiogr*, 1:154–70, 2000.
5. BK Lakatos, Y Nabeshima, M Tokodi, Y Nagata, Z Tösér, K Otani, et al. Importance of nonlongitudinal motion components in right ventricular function: Three-dimensional echocardiographic study in healthy volunteers. *J Am Soc Echocardiogr*, 33:995–1005.e1, 2020.
6. M Tokodi, L Staub, A Budai, BK Lakatos, FI Csákvári, M Suhai, et al. Partitioning the right ventricle into 15 segments and decomposing its motion using 3D echocardiography-based models: The updated ReVISION method. *Front Cardiovasc Med*, 8:622118, 2021.
7. P Mocerri, N Duchateau, S Gillon, L Jaunay, D Baudouy, F Squara, et al. Three-dimensional right ventricular shape and strain in congenital heart disease patients with right ventricular chronic volume loading. *Eur Heart J Cardiovasc Imaging*, 22:1174–81, 2021.
8. A Satriano, P Pournazari, N Hirani, D Helmersen, M Thakrar, J Weatherald, et al. Characterization of right ventricular deformation in pulmonary arterial hypertension using three-dimensional principal strain analysis. *J Am Soc Echocardiogr*, 32:385–93, 2019.
9. J Mitchell, D Mount, and C Papadimitriou. The discrete geodesic problem. *SIAM J Comput*, 16:647–68, 1987.
10. M Di Folco, P Mocerri, P Clarysse, and N Duchateau. Characterizing interactions between cardiac shape and deformation by non-linear manifold learning. *Med Image Anal*, 75:102278, 2022.
11. M Belkin and P Niyogi. Laplacian eigenmaps for dimensionality reduction and data representation. *Neural Comput*, 15:1373–96, 2003.